Supporting Information

Engineered Covalent Organic Framework Nanomotor for Amplified Cuproptosis Therapy via Wnt/β-catenin Signaling Inhibition

Youxian Li,†[a] Yingfei Wang,†[a] Fan Zhou,†[a] Qing Hu,[a] Lingyu Zhong,[a] Junjie Chi,[b] Qing Hao,*[a] and Hong Liu*[a]

[a]State Key Laboratory of Digital Medical Engineering, School of Biological Science and Medical Engineering, Southeast University, Nanjing 210096, China

[b]The First Affiliated Hospital of Wenzhou Medical University, Wenzhou 325035, China

* Corresponding authors.

E-mail: haoq@seu.edu.cn; liuh@seu.edu.cn

Materials

All commercially purchased compounds were used as provided without further purification. Ultrapure water was used in experiments. 1,3,5-tris(4-aminophenyl)benzene (TAPB), benzene-1,3,5-tricarbaldehyde (BTCA) were purchased from Yanshen Technology Co., Ltd (Jilin, China). Acetonitrile (ACN), acetic acid (HAc), tetrahydrofuran (THF), ethanol, 3,3′,5,5′-tetramethylbenzidine (TMB), and 5,5-dimethyl-1-pyrrolidine-N-oxide (DMPO) were purchased from Meryer Chemical Technology Co., Ltd (Shanghai, China). Acetone and dimethyl sulfoxide (DMSO) were purchased from China National Medicines Corporation Ltd. (Beijing, China). Sodium hydroxide (NaOH), copper (II) chloride dihydrate ($CuCl_2 \cdot 2H_2O$), hydrogen peroxide (H_2O_2), and poly(2-hydroxyethyl methacrylate) (pHEMA) were purchased from Sigma-Aldrich Co., Ltd. (Shanghai, China). N-[4-(Aminosulfonyl)phenyl]-4-(3-phenyl-2-propenyl)-1-piperazinecarbothioamide (LF3) was obtained from Bide Pharmatech Ltd. (Shanghai, China), 210 nm mesoporous SiO_2 microspheres were purchased from Nanorainbow Biotech Co., Ltd (Nanjing, China). Bathocuproine disulfonate disodium (BCS), glutathione (GSH), ascorbic acid and Rhodamine 6G (R6G) were purchased from Aladdin Biochemical Technology Co., Ltd. (Shanghai, China).

Dulbecco's modified Eagle's media (DMEM), PBS, pancreatic ferment, and 3-(4,5-dimethylthiazol-2-yl)-2,5-diphenyltetrazolium bromide (MTT) cell proliferation and cytotoxicity assay kit were obtained from KeyGEN Biotech (Nanjing, China). Fetal bovine serum (FBS, 10099141C) was obtained from Thermo Fisher Scientific (California, USA). Annexin V-FITC apoptosis detection kit, mitochondrial membrane potential assay kit with JC-1, C11-BODIPY$^{581/591}$, and Hoechst33342 were purchased from Beyotime Biotech (Shanghai, China). 2′,7′-dichlorofluorescein diacetate (DCFH-DA) was obtained from Sigma-Aldrich Co., Ltd.

(Shanghai, China). β-catenin, ATP7B, DLAT, FDX1, LIAS, and β-actin antibodies were obtained from Proteintech Group, Inc. (Wuhan, China). ATP colorimetric assay kit was purchased from Elabscience Biotech Co., Ltd (Wuhan, China). The bladder cancer cell line murine MB49 was obtained from the National Collection of Authenticated Cell Cultures. Female C57BL/6 mice (8 weeks) were purchased from Jiangsu Qinglongshan Biotech Co., Ltd (Nanjing, China).

Characterization instruments

The morphologies were observed by scanning electron microscope (SEM, Ultra PLUS) and transmission electron microscope (TEM, Talos P200X G2). Powder X-ray diffraction (PXRD) patterns were collected on a SmartL in-situ X-ray diffractometer with Cu Kα radiation (λ=1.5418 Å). Fourier transform infrared (FT-IR) spectra were recorded on a Nicolet IS50 spectrometer. Ultraviolet-visible spectroscopy (UV-Vis) absorbance measurements were recorded on Agilent Cary 60 UV-Vis. X-ray photoelectron spectroscopy (XPS) measurements were performed on an EscaLab 250Xi X-ray photoelectron spectrometer using Al Kα radiation. Cu content was measured by inductively coupled plasma optical emission spectrometer (ICP-OES, Agilent 7850). Dynamic light scattering (DLS) was recorded on Zetasizer Nano ZS90. EPR spectra were recorded on an electron paramagnetic resonance spectrometer (EMXplus-9.5/12). WB analysis was performed on a Gel Imaging System (Syngene). Cell fluorescence images were recorded on a confocal laser scanning microscope (CLSM, Leica SP8). Cytotoxicity assay was recorded on Infinite M200 (TECAN). Cell flow cytometry is performed on a flow cytometer (LongCyte C3140). The laser light source used an 808 nm laser (CNI Laser, MDL-N-808). Thermal imaging pictures were collected on a thermal camera (FLIR E63900). The motor movement behavior was recorded on a metalloscope (BH200M).

The conversion of Cu^{2+} to Cu^{+} mediated by GSH

First, by taking advantage of the specific binding between BCS and Cu^{+}, the characteristic absorption produced at 484nm when Cu^{2+} in a Cu_2SO_4 solution of known concentration (0, 2.5, 5, 10, 15, 20, 25 μM) is converted into Cu^{+} by ascorbic acid and then complexed with BCS is plotted as a standard curve. Subsequently, 100 μg of CP-Motor@LF3 was immersed in 1 mL of PBS (pH 5.8) containing 10 mM GSH, followed by the addition of 10 μL of BCS (100 mM). At predetermined time points (0, 0.5, 1, 2, 4, 8, 16, and 24 min), the absorbance at 484 nm was measured.

Hydroxyl radical (·OH) generation by CP-Motor

CP-Motor (100 μg mL^{-1}) and H_2O_2 (1 mM) were mixed in PBS solution (pH 5.8) and reacted in a water bath at 37℃ for 2 h. Then, 1 mL of the reaction solution was taken and added with 120 μL DMPO (10 mg mL^{-1}) capture agent for EPR testing.

In TMB experiments, the PBS solution (pH 5.8) containing TMB (60 μg mL^{-1}) was mixed with CP-Motor (100 μg mL^{-1}) plus H_2O_2 (1 mM). The generation of ·OH was determined by the absorption increase at 650 nm. The TMB solutions treated with Motor or H_2O alone were used as control groups. After reacting in a 37 °C water bath for 2 h, the absorption spectra were measured. In addition, time-dependent ·OH generation was evaluated by recording the absorbance at 0.5, 1, 1.5, and 2 h. Similarly, TMB experiments were also performed with different concentrations of CP-Motor and different pH levels of PBS.

Photothermal performance testing

150 μg mL^{-1} P-COF dispersed aqueous solution, different concentrations (50, 100, and 150 μg mL^{-1}) of CP-Motor@LF3 dispersed aqueous solution were irradiated respectively under 808 nm near-infrared (NIR) irradiation (1.5 W cm^{-2}) for 10 minutes, and the solution temperatures were recorded with a thermal camera. Similarly, 100 μg mL^{-1} CP-Motor@LF3 was subjected to photothermal testing by irradiating with 808 nm NIR irradiation of different power densities (0.5, 1.0, 1.5, and 2.0 W cm^{-2}) for 10 minutes. Then the group of 1.5 W/cm^2 was selected for four heating and cooling cycle tests.

Intracellular imaging of CP-Motor@LF3

R6G labelled CP-Motor@LF3 was obtained by mixing 4 mL of CP-Motor@LF3 (100 μg mL^{-1}) with 0.5 mL of R6G (200 μM), stirring at room temperature for 24 h, and washing three times with water. 200 μL of MB49 cell suspension (~5×10^4) were seeded in a 4-well confocal dish per well and cultured at 37 °C for 24 h. Each well was incubated with R6G labelled CP-Motor@LF3 (200 μL, 20 μg/mL) with 808 nm NIR light irradiation (1.5 W cm^{-2}) for 10 min, subsequently washed with PBS thoroughly three times to remove uninternalized CP-Motor@LF3. MB49 cells were subsequently stained with Hoechst 33258 (200 μL, 1 μM) for 30 min to indicate the cell nucleus, and the co-localization of R6G fluorescence and Hoechst 33258 fluorescence was monitored with CLSM.

Cell apoptosis analysis

Cell apoptosis induced by CP-Motor@LF3 was evaluated by Annexin V-FITC apoptosis detection kit using flow cytometry. 5×10^5 MB49 cells were seeded in a 6-well plate per well and cultured at 37 °C for 24 h, subsequently treated with PBS, Motor@LF3, CP-Motor, and CP-Motor@LF3 (1.25 μg mL^{-1}), respectively, for another 24 h. Afterwards, MB49 cells in each well were collected and washed three times with PBS, subsequently stained with 5 μL Annexin V-FITC and 10 μL propidium iodide at room temperature for 15 min in dark conditions, followed by flow cytometry to identify the apoptotic cells.

MTT assay

MTT assay was performed to quantitatively evaluate the therapeutic effect of CP-Motor@LF3 in vitro. MB49 cells were seeded in a 96-well plate at a density of 5000 cells per well and incubated at 37 °C for 24 h. Subsequently, 100 μL of PBS, Motor@LF3, CP-Motor, and CP-Motor@LF3 were added into each well and co-cultured for 24 h, respectively. PBS treated MB49 cells as a control. Afterwards, 50 μL of 1×MTT solution was added to each well and incubated with MB49 cells for 4 h to test cell viability. After removing the remaining MTT solution, the produced formazan precipitates were dissolved in 150 μL DMSO, and the absorbance was measured at 492 nm with a microplate reader.

Observation of DLAT oligomerization under fluorescence microscopy

MB49 cells (5×10^5 cells/well) were seeded into a 6-well plate and cultured for 24 h. After that, the cells were treated with PBS, Motor@LF3, CP-Motor, and CP-Motor@LF3 (10 μg mL^{-1}) for 12 h. Thereafter, the cells were washed three times with PBS and fixed with 4% paraformaldehyde for immunostaining. Next, the cells were incubated with the DLAT antibody at 4 °C overnight, treated with secondary antibody at room temperature for 1 h, stained with DAPI for 15 min, and imaged under a fluorescence microscopy.

Evaluation of mitochondrial membrane potential

MB49 cells were seeded into a single chamber confocal dish of 5×10^5 cells per confocal dish and cultured for 24h. The cells were then treated with PBS, Motor@LF3, CP-Motor, and CP-Motor@LF3 (10 μg mL^{-1}) for 24h, respectively. For the mitochondrial membrane potential assay, the cells were stained with the JC-1 staining working solution as well as Hoechst 33258 (1 μM) and observed by CLSM.

Intracellular ATP detection

5×10^5 MB49 cells were seeded in a 6-well plate per well and incubated at 37 °C overnight, subsequently treated with PBS, Motor@LF3, CP-Motor, and CP-Motor@LF3 (10 μg mL^{-1}), respectively, and further incubated for 24 h. Finally, the cells were collected, and the intracellular ATP content was measured using an ATP colorimetric assay kit.

Histopathology analysis

For Hematoxylin and Eosin (H&E) staining, the heart, liver, spleen, lung, kidney, and tumor of mice from the five groups were harvested and fixed in 4% paraformaldehyde, then embedded in paraffin. The paraffin-embedded tissues were then cut into slices and stained with hematoxylin and eosin for observation with an optical microscope. In addition, tumors of mice from the five groups were stained for TUNEL and ki-67 using the above methods.

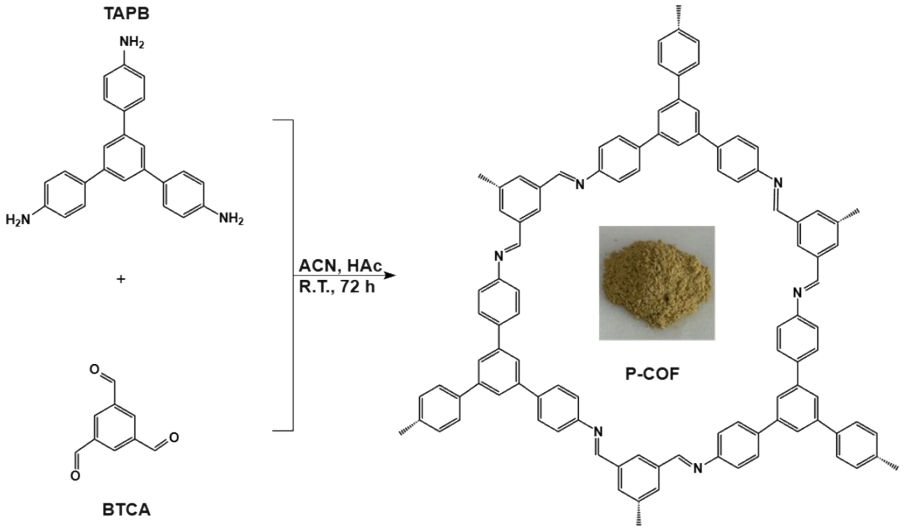

Figure S1. The synthesis diagram of COF nanospheres (P-COF) and P-COF products (inset).

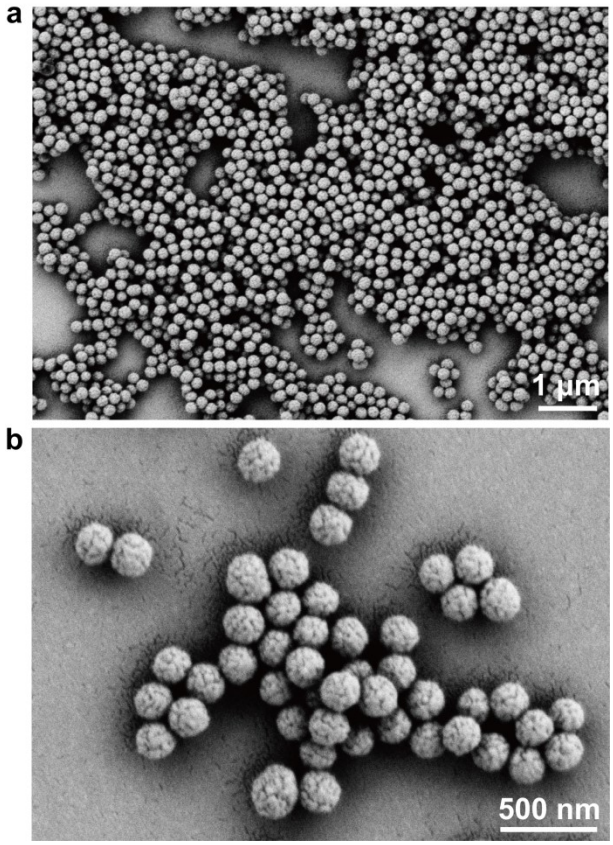

Figure S2. SEM images of P-COF at different scales.

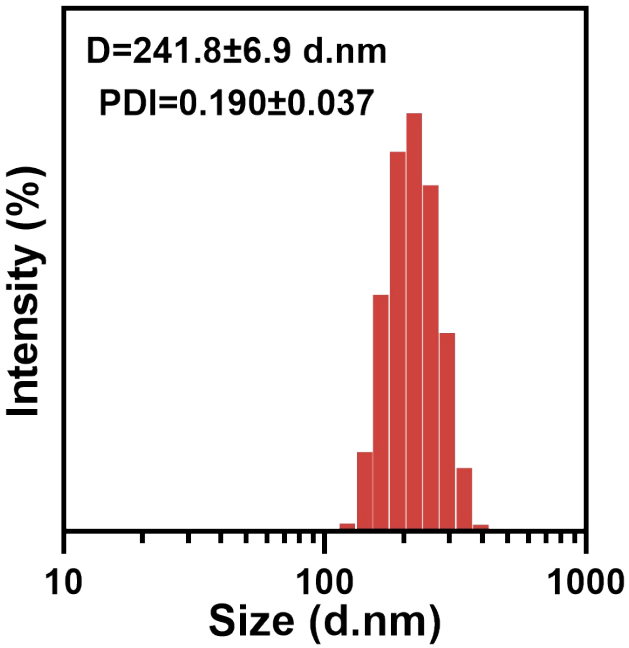

Figure S3. Hydrated particle size of P-COF.

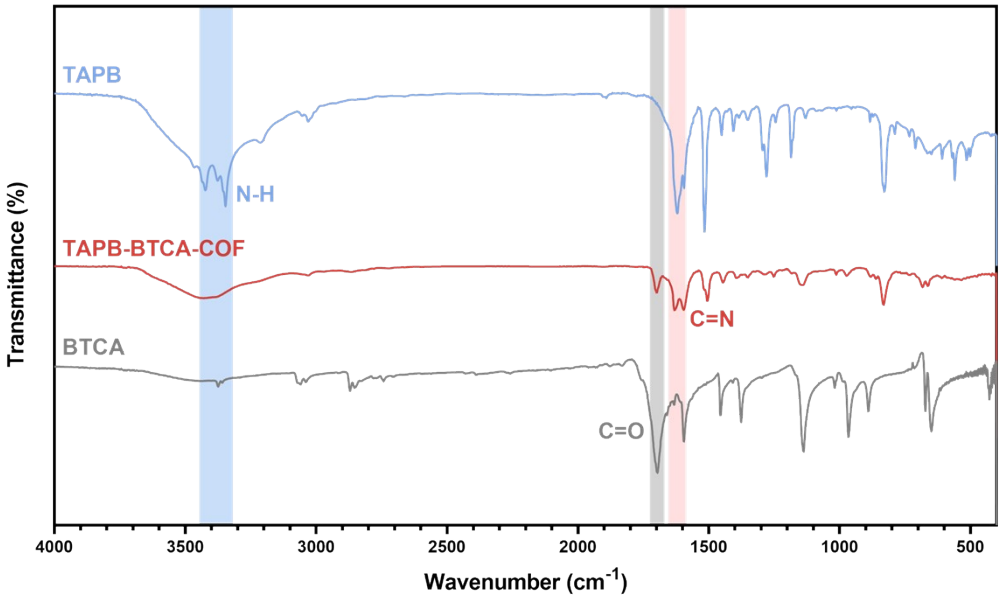

Figure S4. FT-IR spectra of TAPB, P-COF, and BTCA.

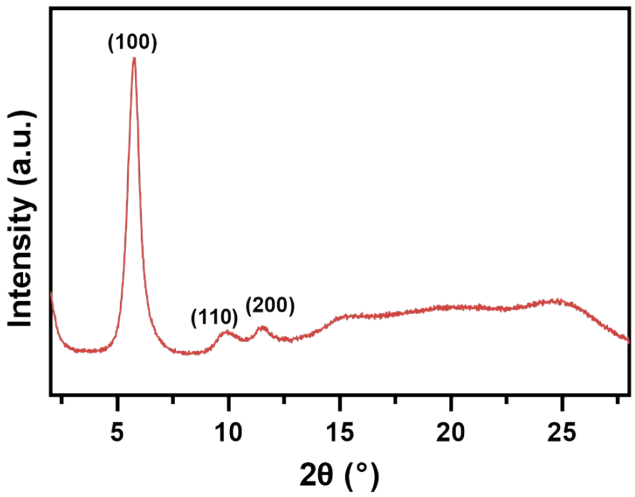

Figure S5. PXRD pattern of P-COF.

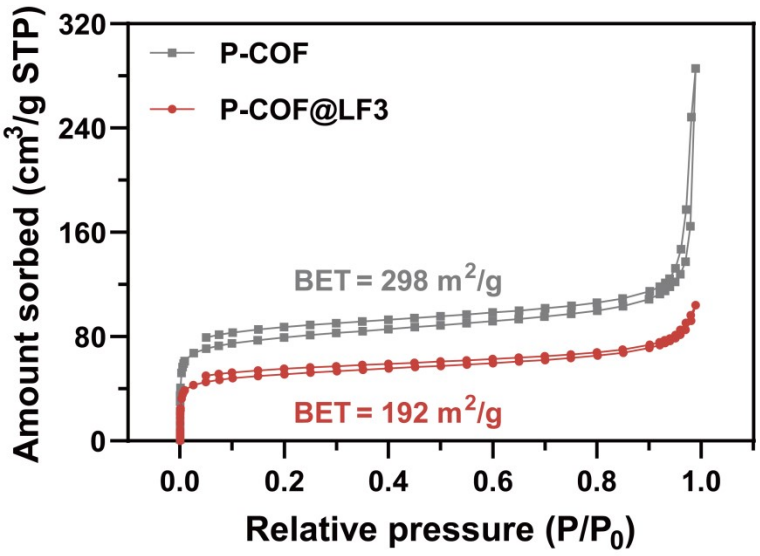

Figure S6. N_2 adsorption-desorption isotherms of P-COF before and after loading LF3.

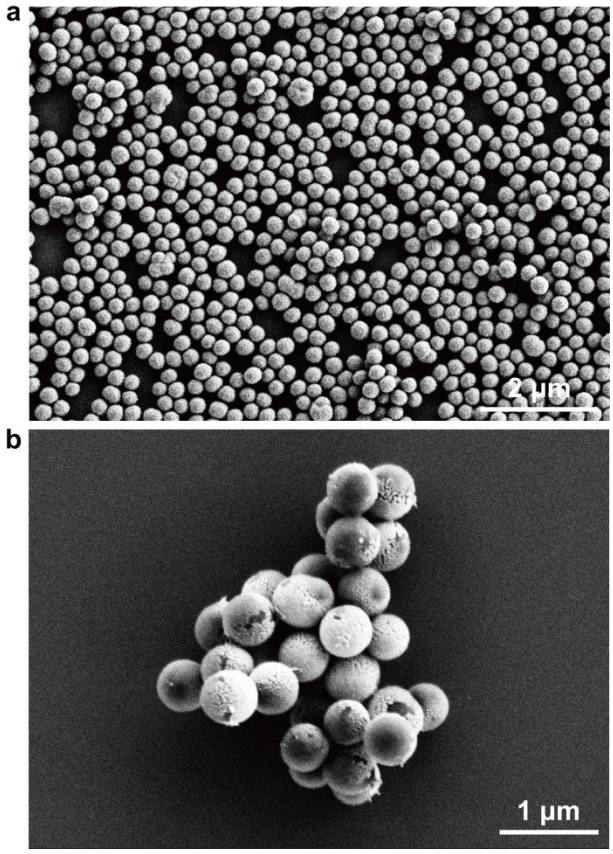

Figure S7. SEM images of (a) a monolayer of P-COF and (b) Motor.

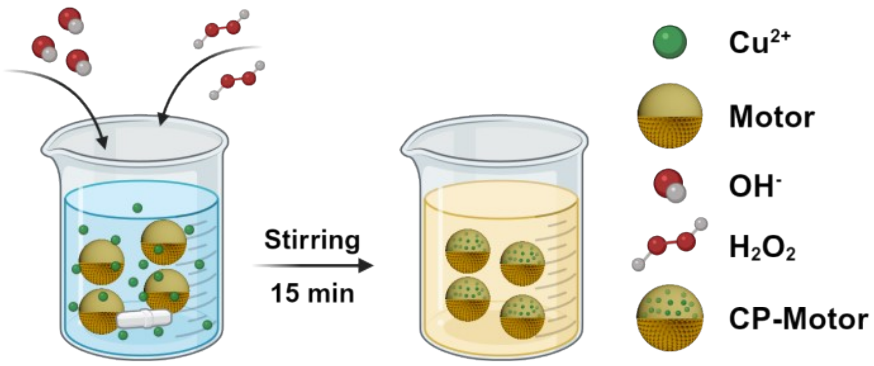

Figure S8. Schematic illustration of the synthetic process of CP-Motor.

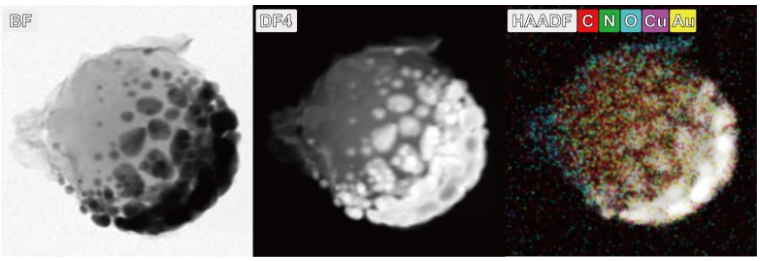

Figure S9. Energy dispersive X-ray (EDX)-mapping images of CP-Motor.

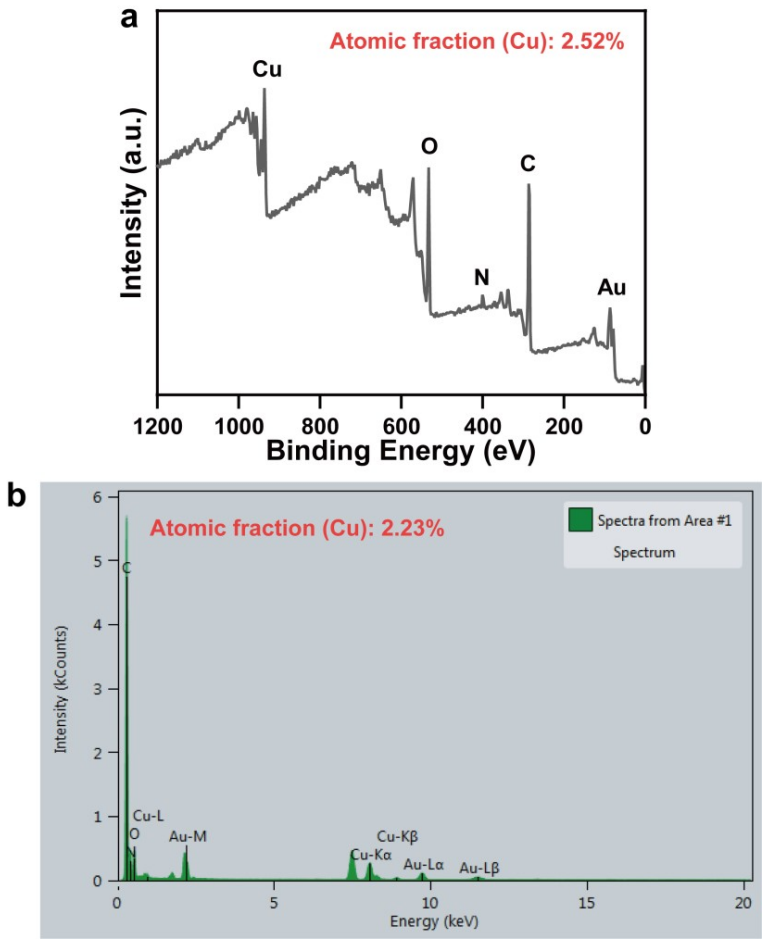

Figure S10. (a) Survey XPS spectra and (b) EDX spectral analysis of CP-Motor.

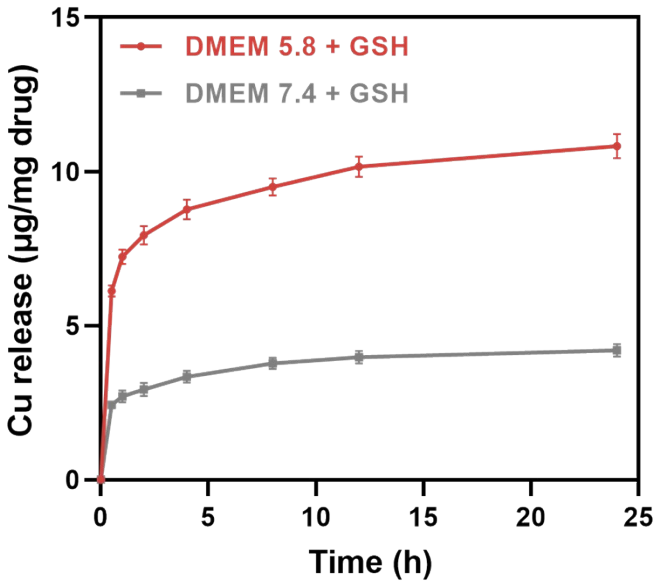

Figure S11. Cumulative Cu release from CP-Motor in DMEM at different pH in the presence of 10 mM GSH.

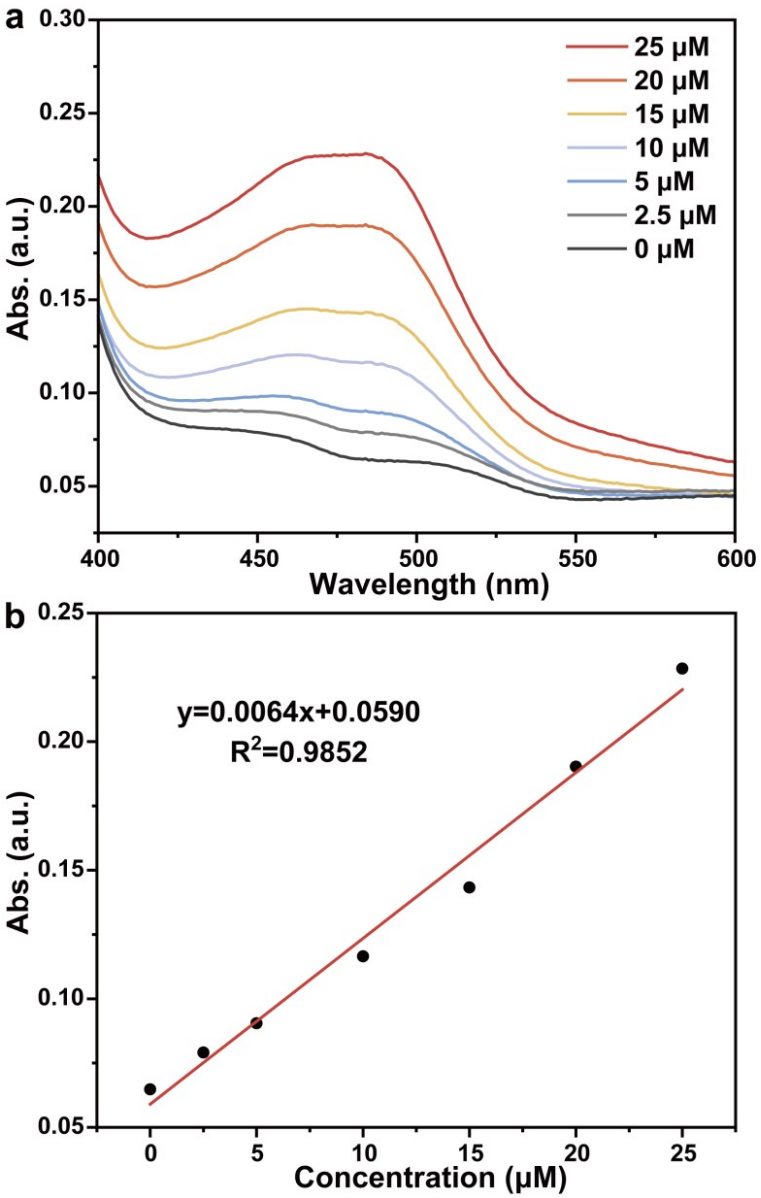

Figure S12. (a) UV-Vis absorption spectra of the BCS-Cu^{+} complex with different concentrations of Cu^{+}. (b) The corresponding standard curve of absorbance at 484 nm versus Cu^{+} concentration.

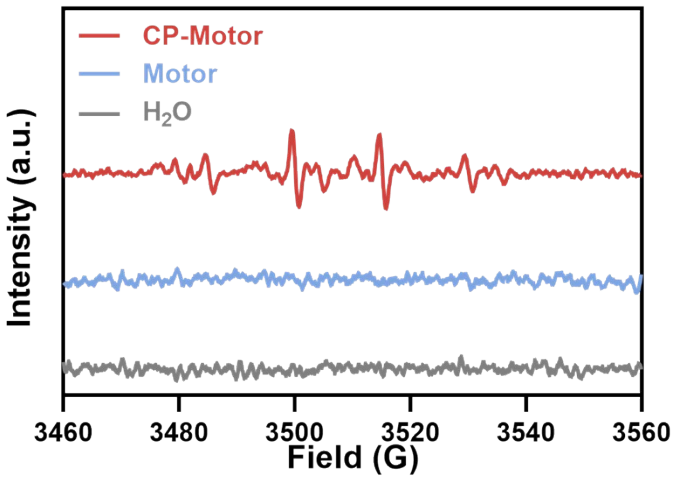

Figure S13. EPR spectra of DMPO, H_2O_2 with CP-Motor and Motor at pH 5.8.

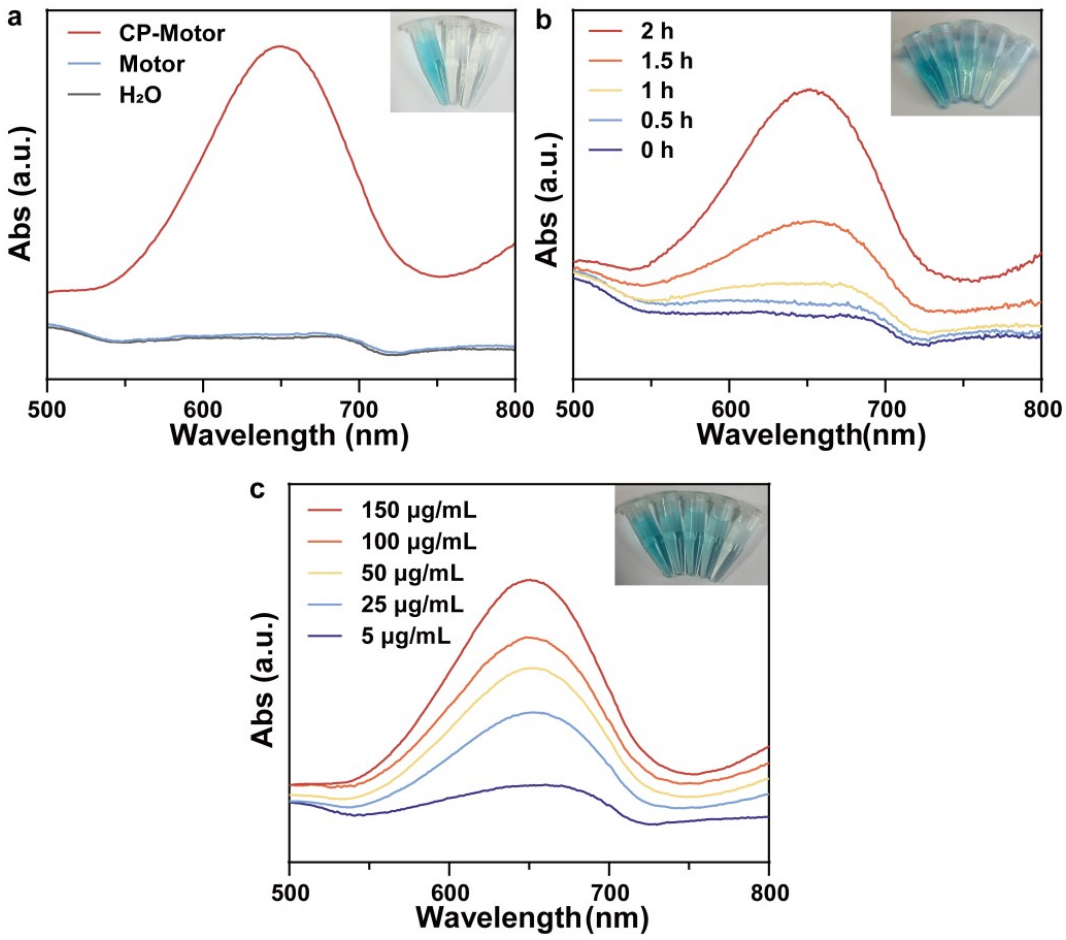

Figure S14. (a) UV-Vis absorption spectra and photographs (inset) of TMB treated with CP-Motor, Motor, and H_2O for 2 h under acidic conditions (pH 5.8). (b) UV-Vis absorption spectra and photographs (inset) of TMB treated with CP-Motor under acidic conditions (pH 5.8) recorded at different time points (0, 0.5, 1, 1.5, and 2 h). (c)UV-Vis absorption spectra and photographs (inset) of TMB treated with different concentrations of CP-Motor for 2 h under acidic conditions (pH 5.8).

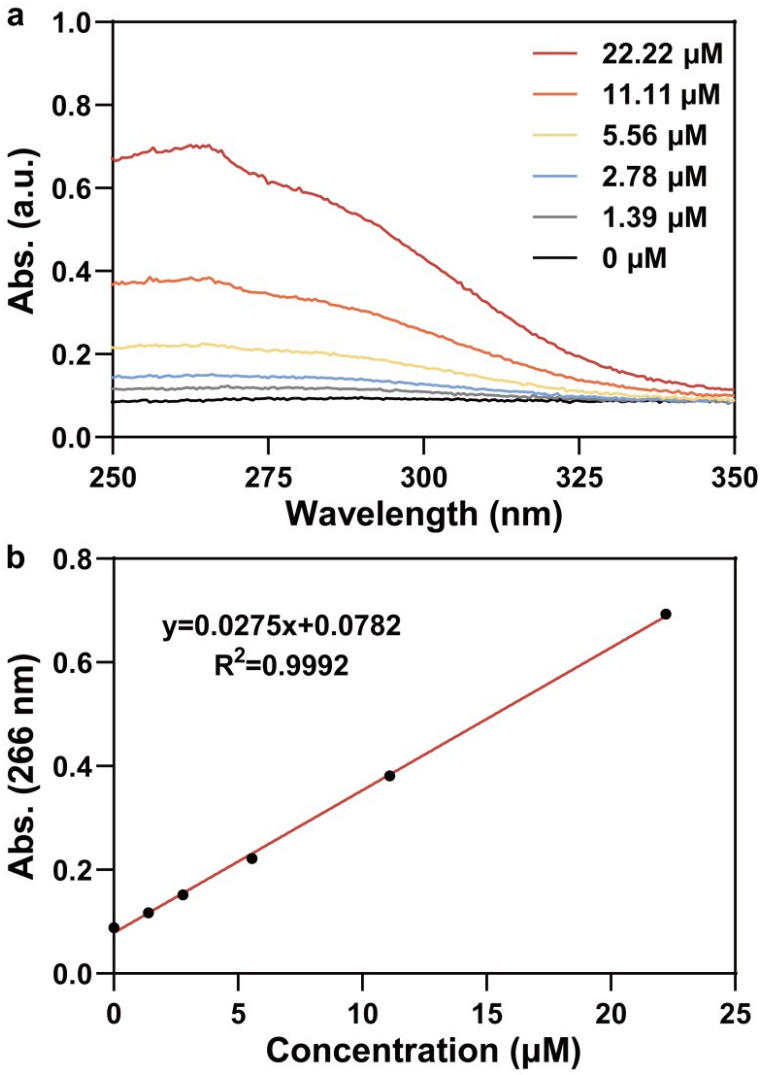

Figure S15. (a) UV-Vis spectra of LF3 at different concentrations. (b) The standard curve of absorbance at 266 nm versus concentration of LF3.

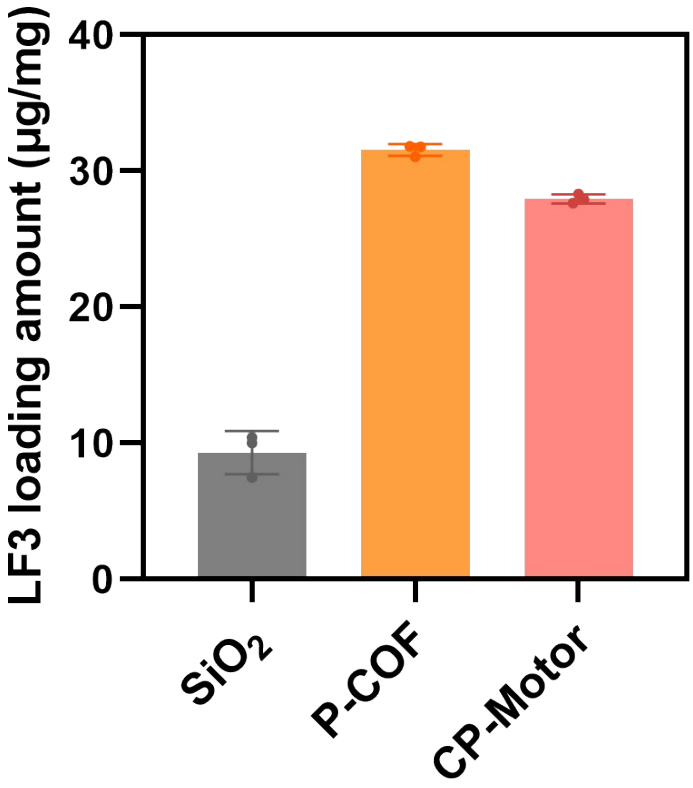

Figure S16. LF3 loading amounts on different carriers. Error bars indicate means ± SD (n = 3).

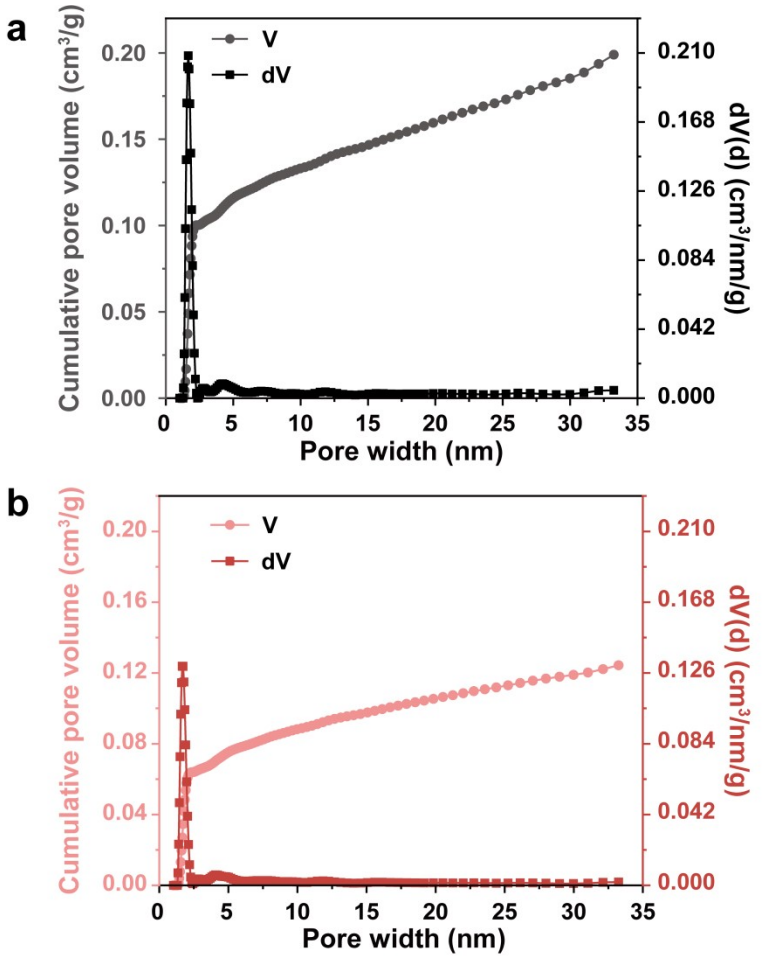

Figure S17. Cumulative pore volume curves and pore size distributions of (a) P-COF and (b) P-COF@LF3.

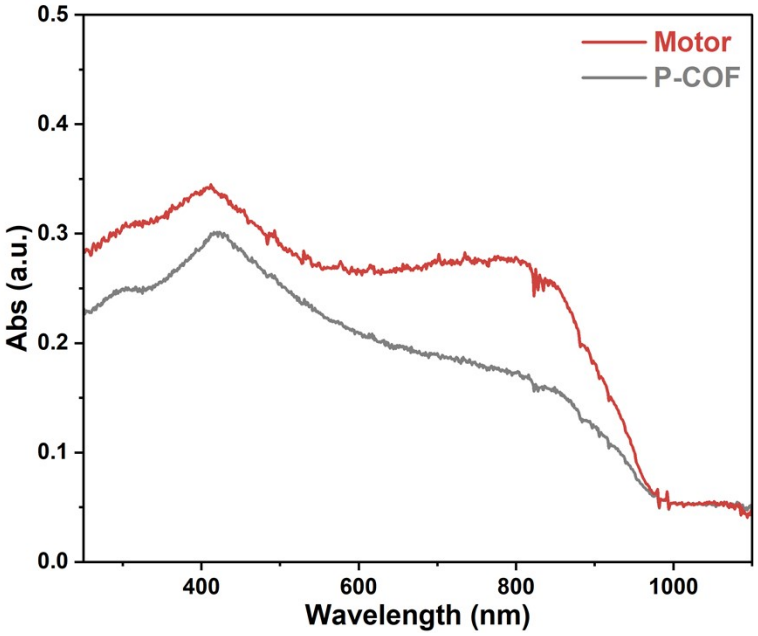

Figure S18. UV-vis absorption spectra of Motor. P-COF was set as the control.

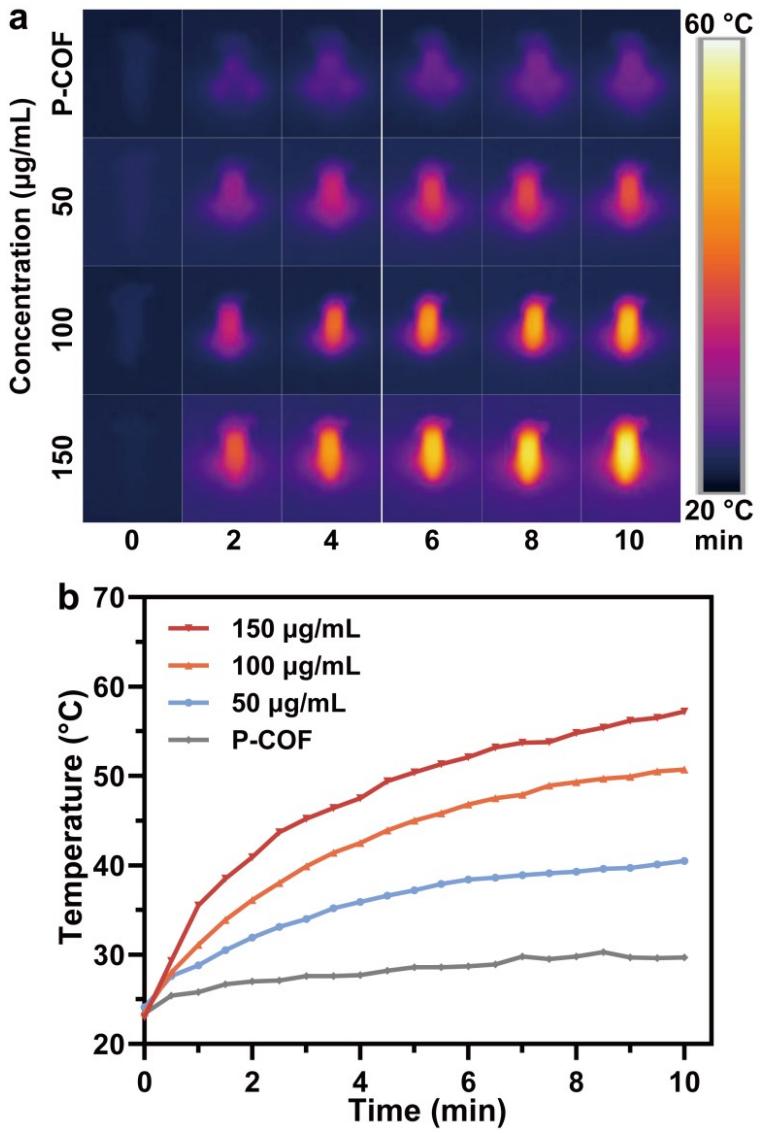

Figure S19. (a) Infrared thermal images and (b) photothermal heating curves of various concentrations of CP-Motor@LF3 (50, 100, 150 μg mL^{-1}) and P-COF (150 μg mL^{-1}) as a control set upon exposure to 808 nm laser for 10 min at a power of 1.5 W cm^{-2}.

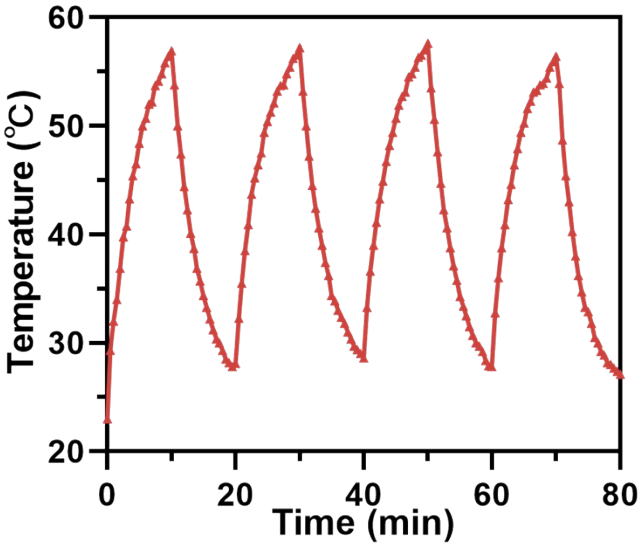

Figure S20. Photothermal stability of CP-Motor@LF3 upon 808 nm laser irradiation of 1.5 W cm^{-2} for four on/off cycles.

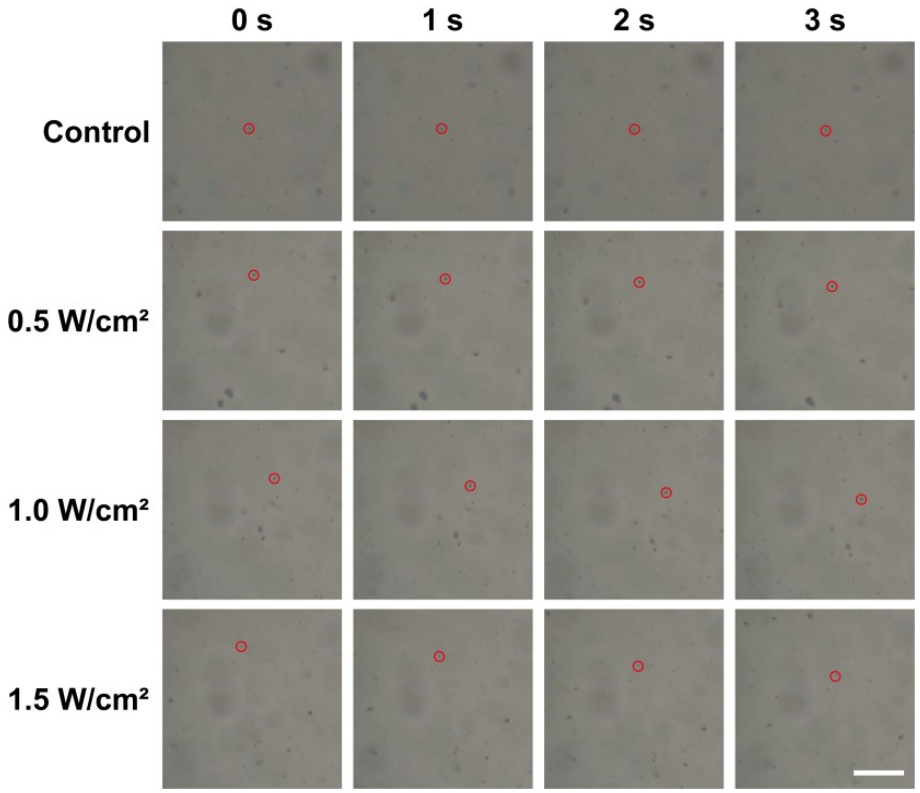

Figure S21. Time-lapsed images of CP-Motor@LF3 in PBS (control) and under NIR irradiations of 0.5, 1.0, and 1.5 W cm^{-2}, respectively (scale bar: 50 μm).

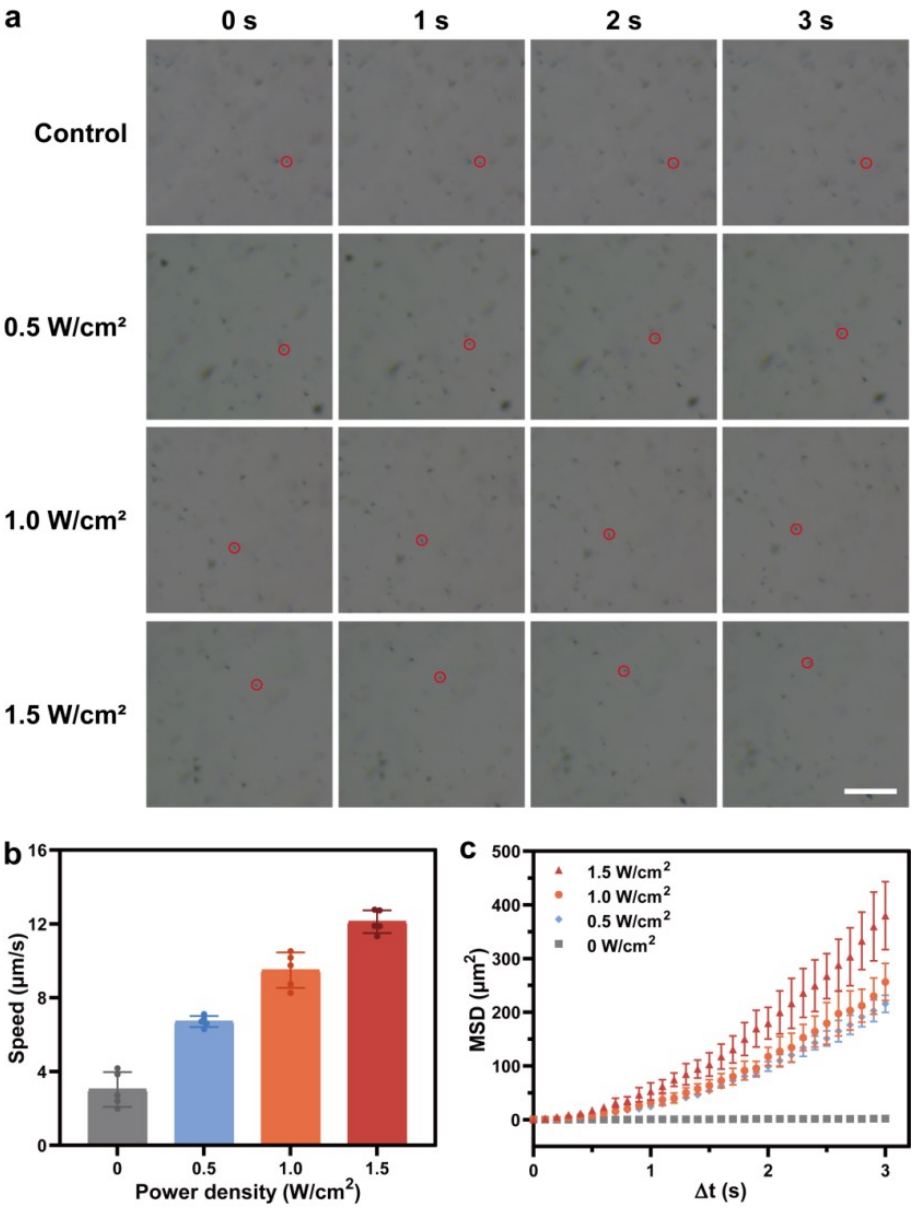

Figure S22. (a) Time-lapsed images of CP-Motor@LF3 in cell culture media supplemented with 10% FBS (control) and under NIR irradiation of 0.5, 1.0, and 1.5 W cm^{-2}, respectively (scale bar: 50 μm), and corresponding (b) motion speeds and (c) MSD plots (3 s). Error bars indicate means±SD (n=5).

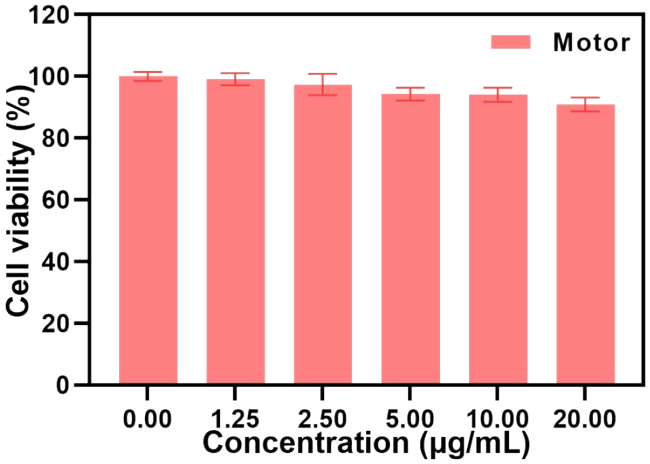

Figure S23. Cell viability of MB49 cells treated with Motor.

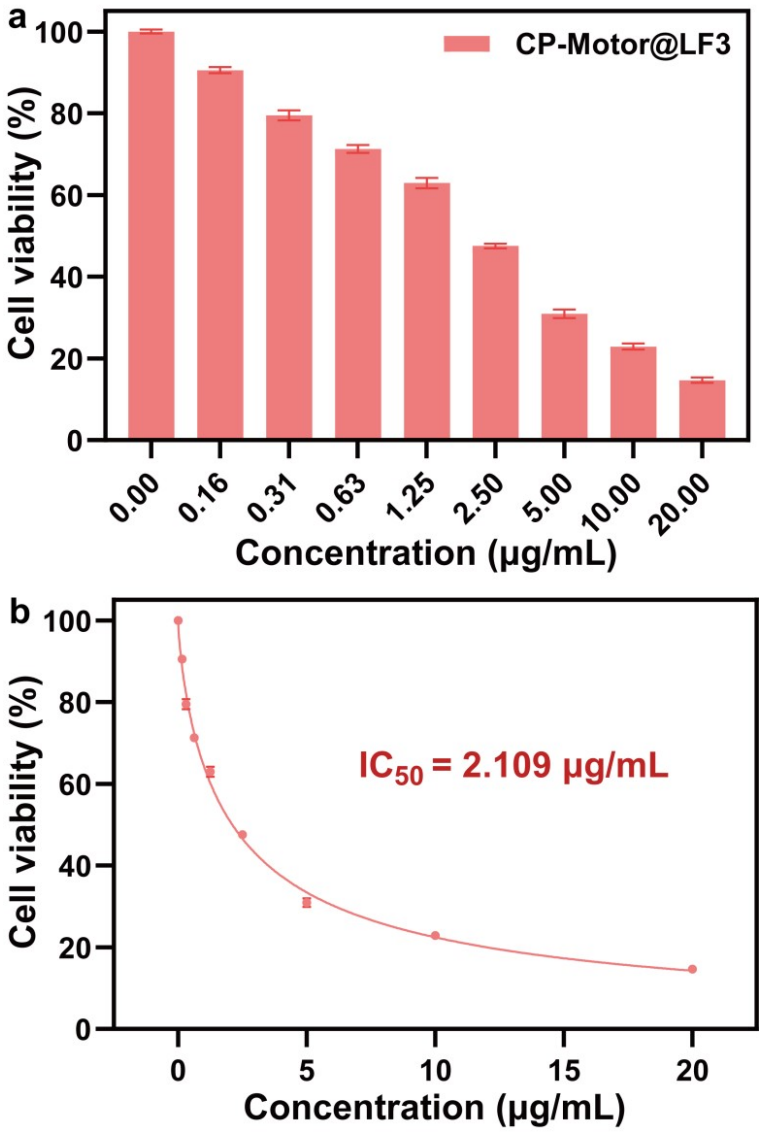

Figure S24. (a) Cell viability of MB49 cells treated with different concentrations of CP-Motor@LF3 (0 to 20 μg mL^{-1}), and corresponding (b) IC_{50} level of CP-Motor@LF3.

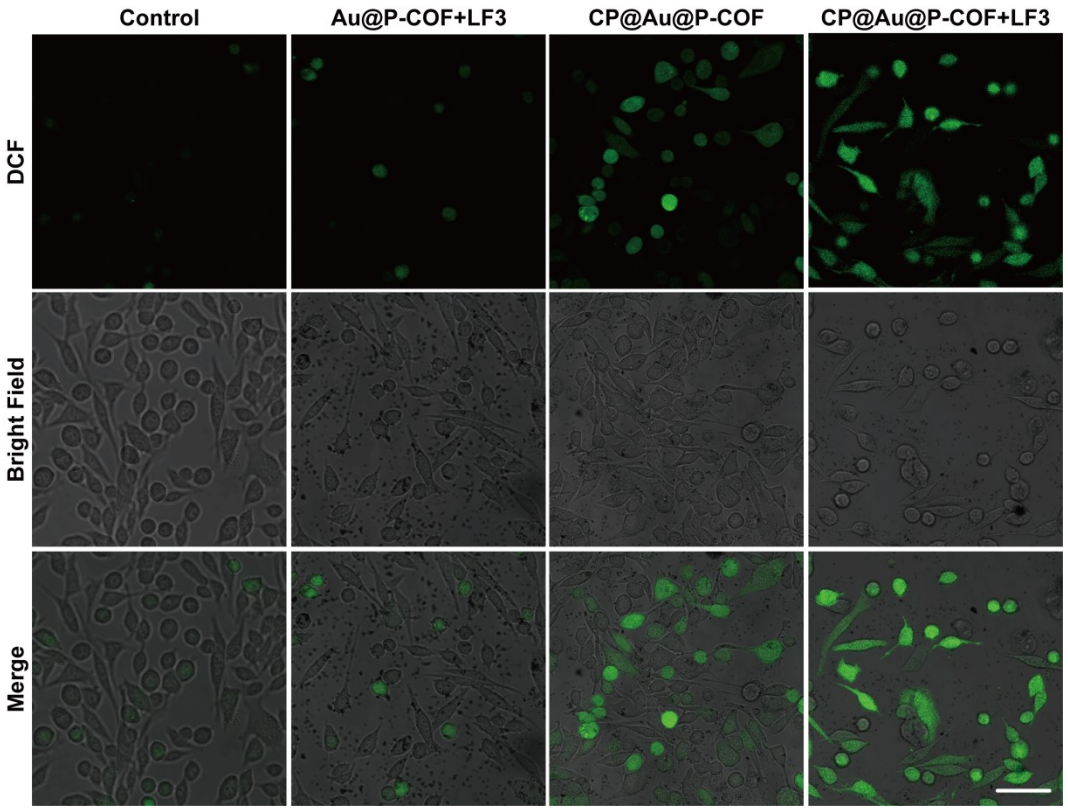

Figure S25. Fluorescence images of intracellular DCF fluorescence intensities (scale bar: 50 μm).

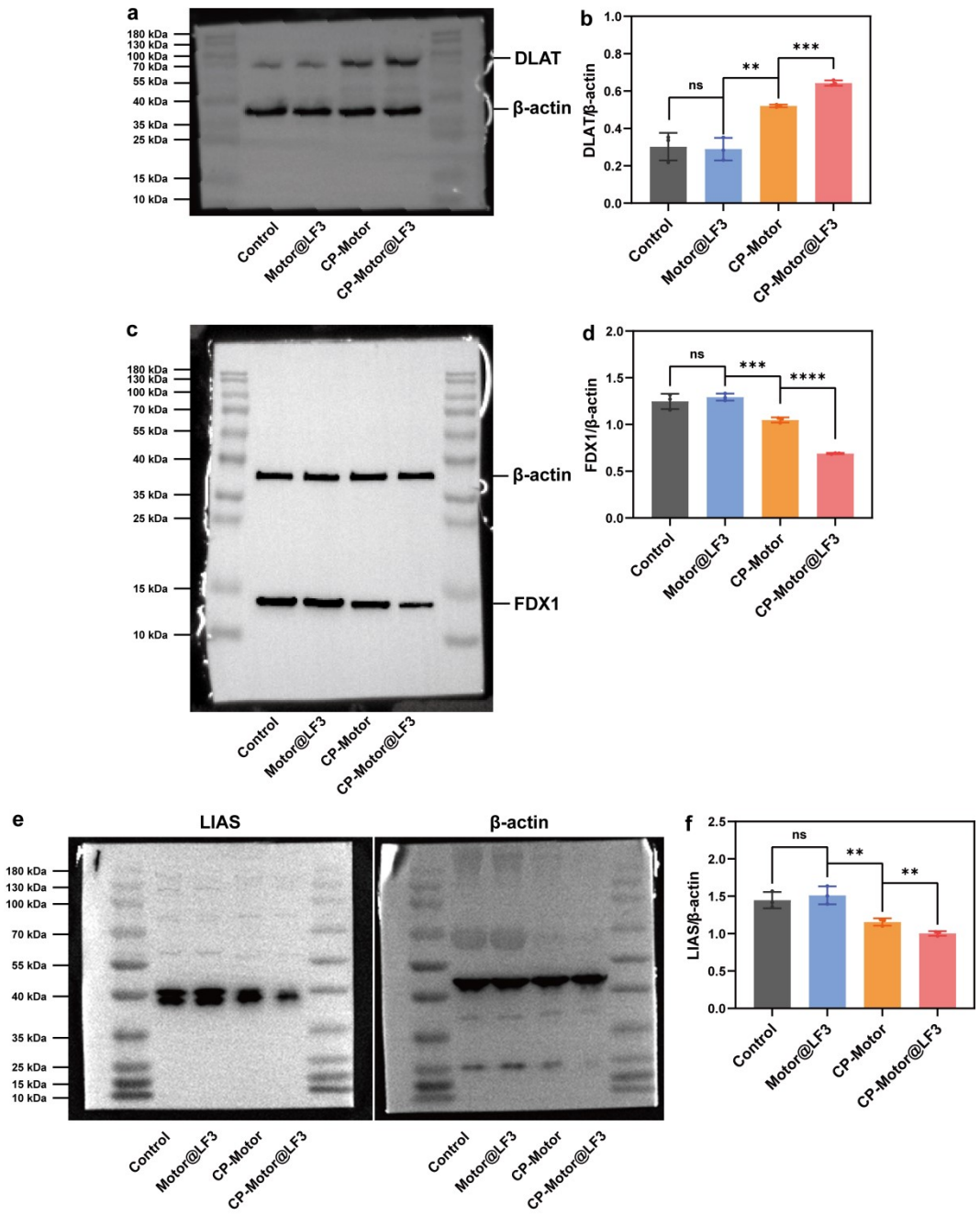

Figure S26. (a, b) Uncropped/full-size western blots and relative grey value for DLAT (69-70 kDa) after different treatments. (c, d) Uncropped/full-size western blots and relative grey value for FDX1 (14 kDa) after different treatments. (e, f) Uncropped/full-size western blots and relative grey value for LIAS (34-42 kDa) after different treatments.

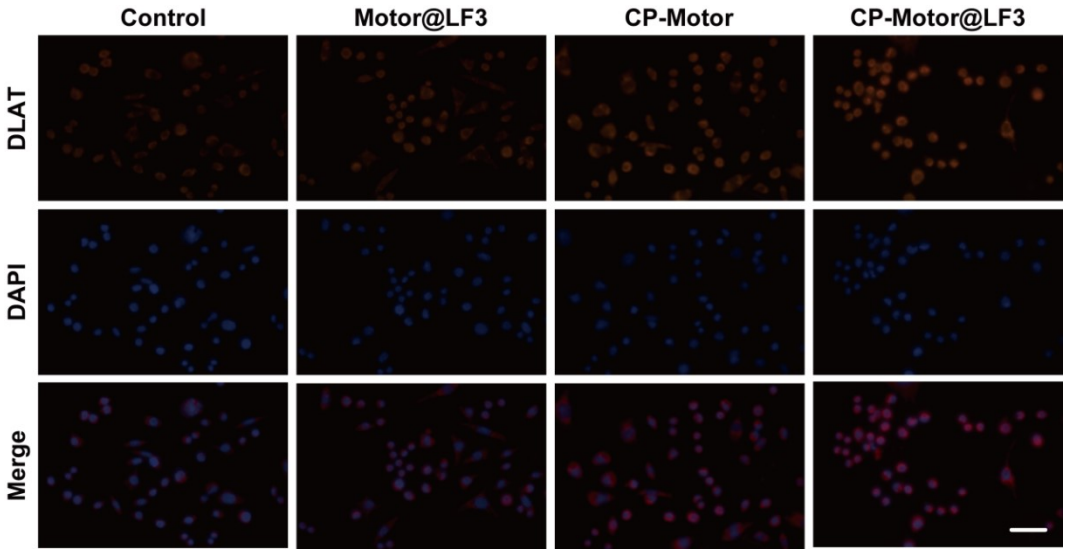

Figure S27. Immunofluorescence analysis of DLAT in MB49 cells after different treatments (scale bar: 50 μm).

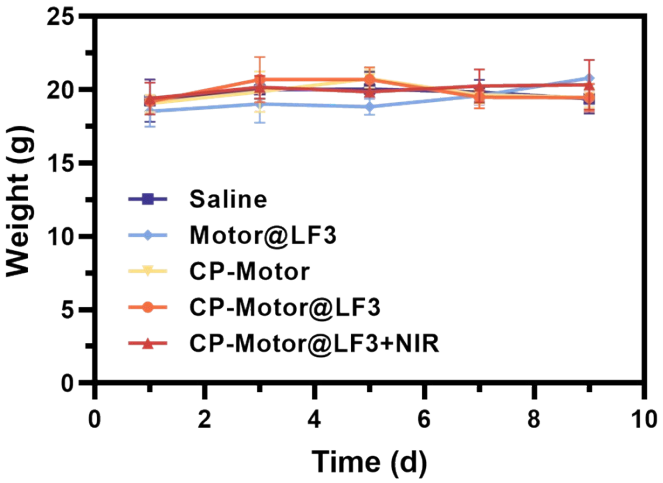

Figure S28. Body weight curves of the MB49 tumor-bearing mice after different treatments.

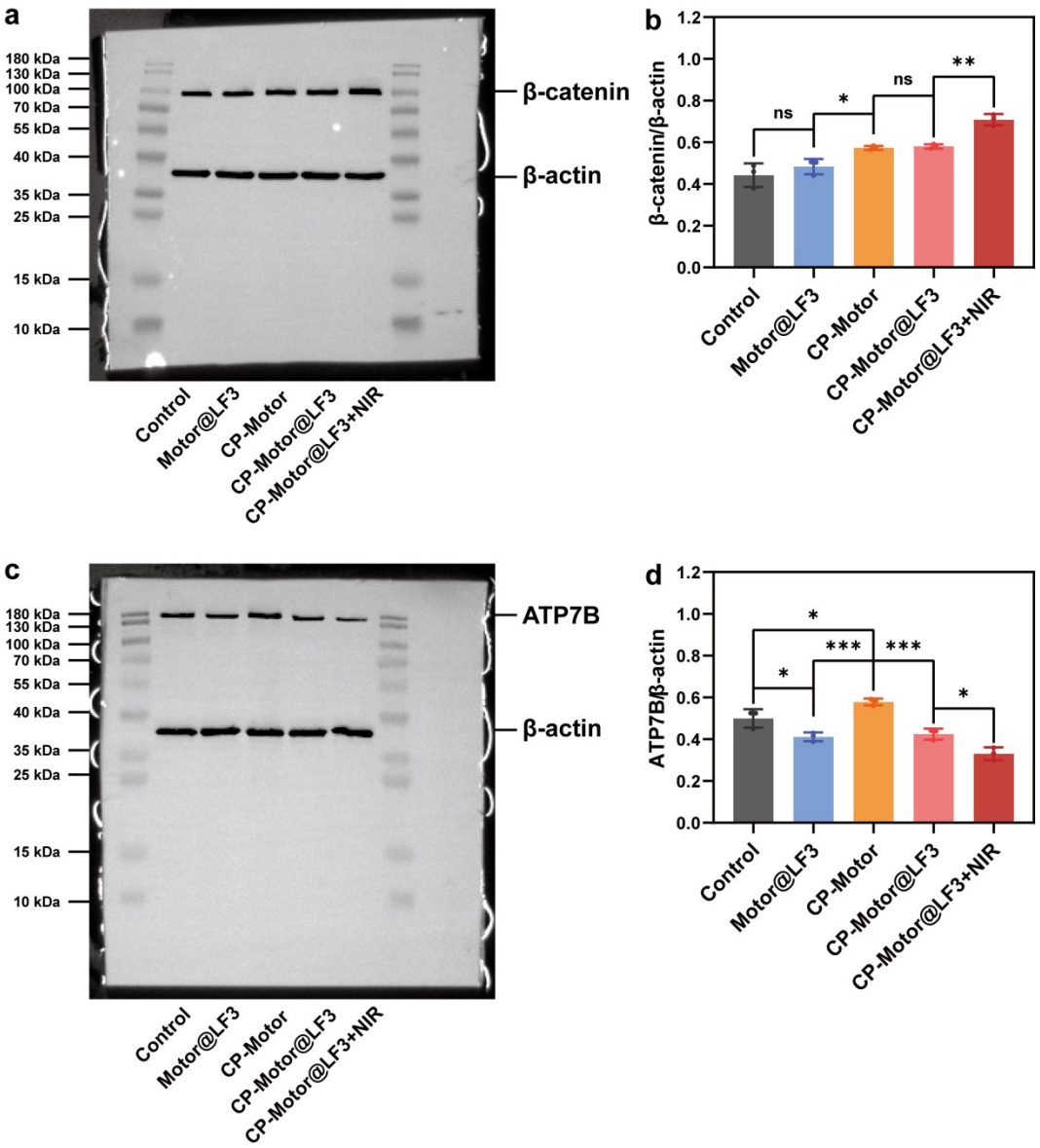

Figure S29. (a, b) Uncropped/full-size western blots and relative grey value for β-catenin (92 kDa) after different treatments. (c, d) Uncropped/full-size western blots and relative grey value for ATP7B (157 kDa) after different treatments.

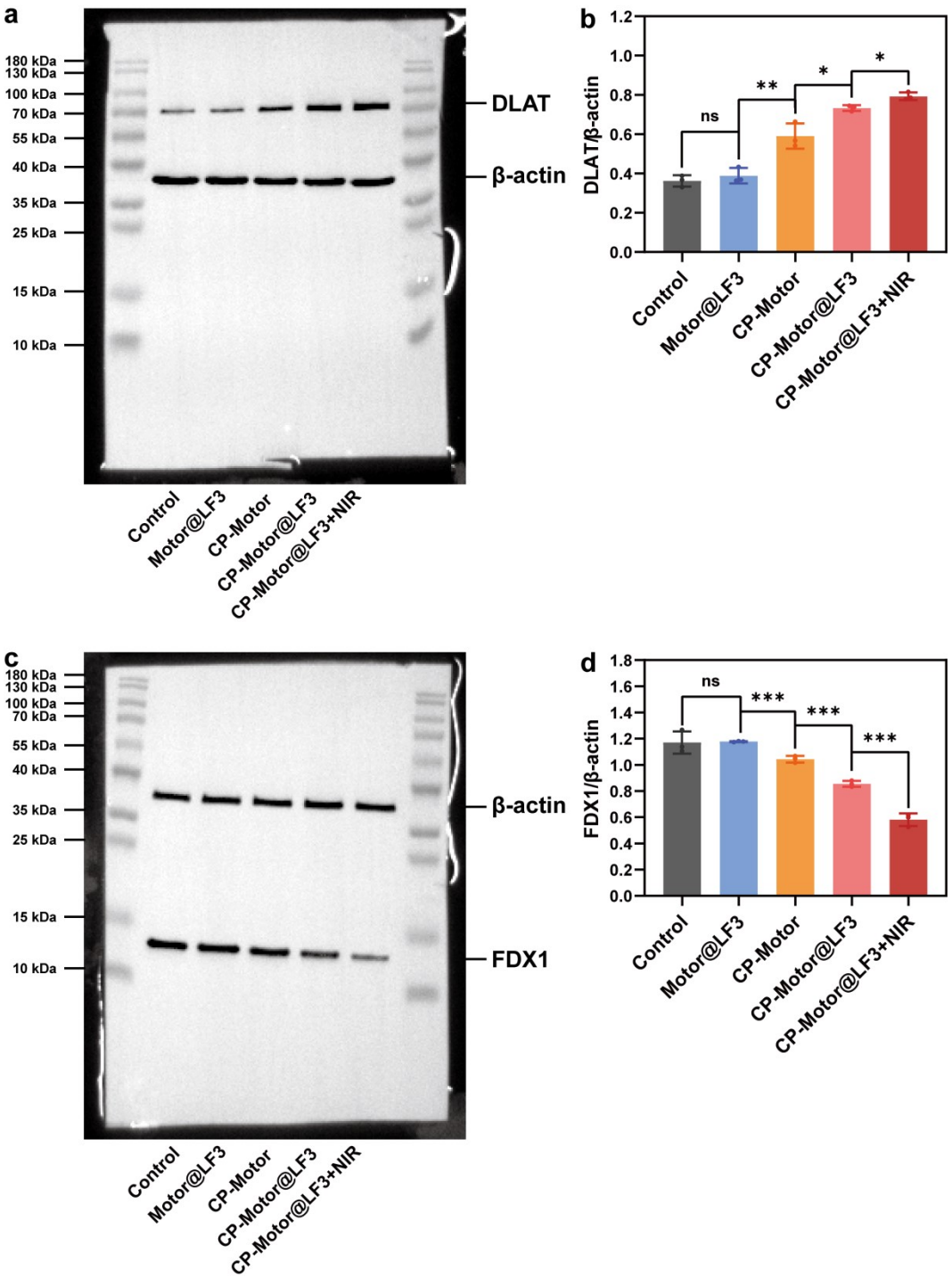

Figure S30. (a, b) Uncropped/full-size western blots and relative grey value for DLAT (69-70 kDa) after different treatments. (c, d) Uncropped/full-size western blots and relative grey value for FDX1 (14 kDa) after different treatments.

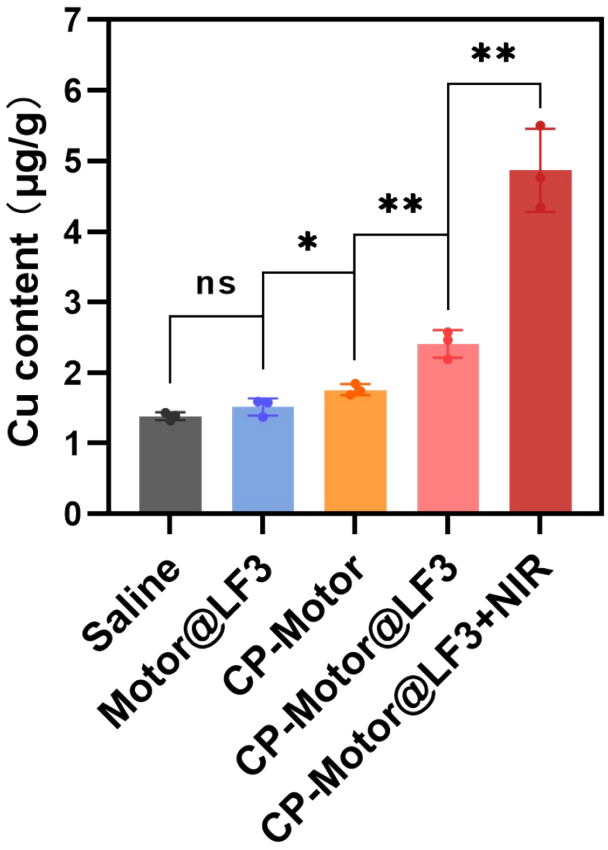

Figure S31. ICP-OES analysis of copper content in tumor tissues from different treatment groups.

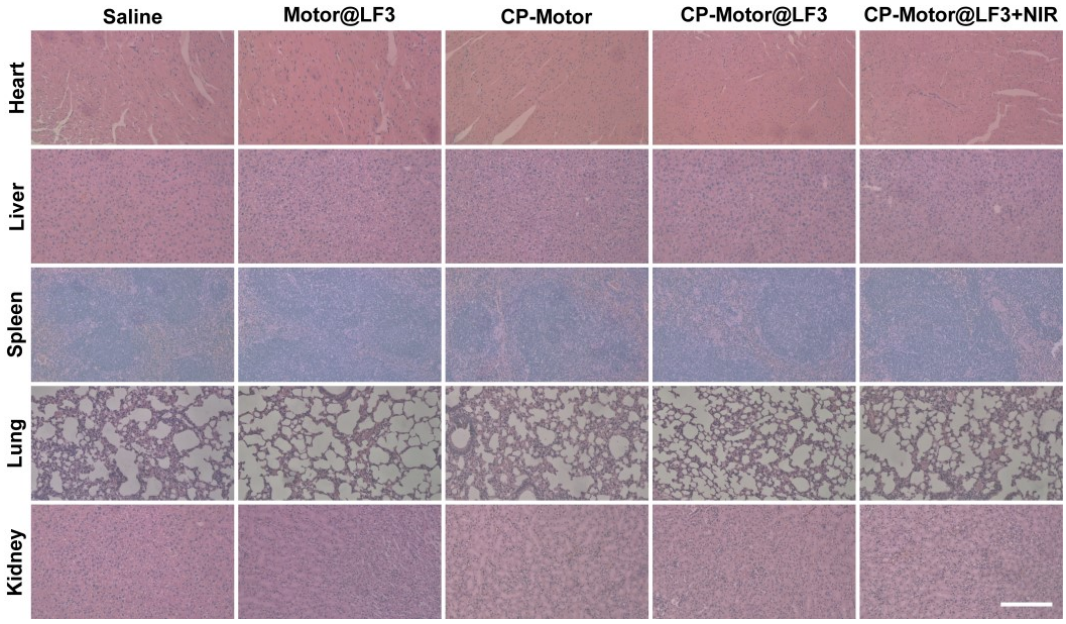

Figure S32. H&E staining of heart, liver, spleen, lung, and kidney of mice on Day 9 after various treatments (scale bar: 100 μm).